ORGANIC CHEMISTRY FRONTIERS

CCS 中国化学会 CHINESE CHEMICAL SOCIETY

SIOC

ROYAL SOCIETY OF CHEMISTRY

Transformation of benzocorrole isomer into pyrrole-containing polycyclic molecules via copper-mediated cleavage and annulation

Journal:	*Organic Chemistry Frontiers*
Manuscript ID	QO-RES-11-2024-002145.R1
Article Type:	Research Article
Date Submitted by the Author:	09-Dec-2024
Complete List of Authors:	Basumatary, Biju; Kyushu University Yada, Sawako; Kyushu University Oka, Shunsuke; Tokyo Metropolitan University Mori, Shigeki; Ehime University Mori, Tatsuya; Kyushu University Abe, Tatsuki; Kyushu University Kawaguchi, Daisuke; Kyushu University Yasuda, Takuma; Kyushu University Furuta, Hiroyuki; Kyushu University Ishida, Masatoshi; Tokyo Metropolitan University

ARTICLE

Transformation of benzocorrole isomer into pyrrole-containing polycyclic molecules via copper-mediated cleavage and annulation

Received 00th January 20xx,
Accepted 00th January 20xx

DOI: 10.1039/x0xx00000x

Biju Basumatary,[#,a] Sawako Yada,[#,a] Shunsuke Oka,[b] Shigeki Mori,[c] Tatsuya Mori,[d] Tatsuki Abe,[a] Daisuke Kawaguchi,[a] Takuma Yasuda,*[d] Hiroyuki Furuta*[a] and Masatoshi Ishida*[b]

We present the oxidative transformation of a corrole isomer, namely, dibenzocorrorin (**3**), featuring a modified connectivity pattern of bipyrrole moieties within the corrole scaffold, resulting in the formation of pyrrole-embedded polycyclic molecules (**1** and **2**). The X-ray crystallography analysis of compound **1** revealed the establishment of three C–N bonds through nitrogen sites in the pyrrole and indole rings, leading to a highly π-conjugated core with nine fused aromatic rings. Notably, the β-pyrrole protons of the diazadicyclopentaazulene moiety displayed significant high-field shifts in the ^{1}H-NMR spectrum, attributed to the 12π antiaromatic contribution of the diazadicyclopentaazulene segment, as indicated by NICS and ACID plot analyses. Compound **1** exhibited a broad near-infrared absorption beyond 1000 nm, a narrow electrochemical energy gap (ΔE = 1.15 V), a short excited-state lifetime, and stable photothermal conversion capability. The crystalline packing structure of **1**, characterized by a staircase-like stacking along the long axis of needle-shaped crystals, facilitated the fabrication of a single-crystal organic field-effect transistor. The resulting device demonstrated p-type semiconductor behaviour, emphasizing the potential of **1** in near-infrared optoelectronic applications.

Introduction

The "destruction and mutation" of critical molecular skeletons generate functional diversity, which is essential in the evolution of materials. In this context, porphyrins are well-known cyclic π-conjugated molecules, widely recognized as key structural motifs in functional materials due to their exceptional chemical stability, distinctive optical and electrochemical properties, excellent biocompatibility, and versatile metal-coordination abilities.[1] In particular, the macrocyclic structures of porphyrins and related molecules play specific roles in various material applications such as catalysis, sensing, medicinal therapies, and supramolecular assemblies.[2] Therefore, to explore novel properties and functions of porphyrin-related macrocycles, the structural modification of the parent tetrapyrrolic scaffolds using unique synthetic techniques has attracted significant attention. Among the analogues, ring-contracted porphyrinoids, such as corroles, are fully conjugated corrins with one less *meso*-carbon atom than their parent porphyrins.[3] The removal of this carbon atom from the porphyrin scaffold results in a redox-active (non-innocent) macrocycle with distinctive oxidative reactivity. Furthermore, the breakdown of the macrocyclic skeleton via oxygenation-induced ring-opening reactions has been identified as a critical method for creating novel π-skeletons.[4] However, the open-chain corrole skeleton has been less studied compared to porphyrin congeners (Fig. 1a).[5]

In this work, we report a novel π-conjugated corrole isomer, named corrorin, composed of an α,β-linked bipyrrole unit that demonstrates unique oxidative ring-opening and subsequent fusion reactions. In a one-pot process, these reactions afford multiply fused polycyclic molecules (**1** and **2**) (Fig. 1c and 2a). Due to the intrinsic 18π aromatic stabilization feature, the corrole scaffold is typically stable, thereby making breaking specific C–C bonds difficult and rearranging the tetrapyrrole structure to form open-chain products.[6] In contrast, the highly strained and twisted bipyrrole moiety in the nonaromatic corrorin core is relatively unstable (ΔE = 22.9 kcal mol^{-1}) compared to that of the aromatic corrole congener. The specific C–C bond order index of the bipyrrole moiety in the corrorin was calculated to be 1.0514, which is relatively smaller than that of corrole (1.2090) by natural bond orbital (NBO) analysis (Fig. 1d).[7] These theoretical results suggest it may serve as a potential molecular platform for reconstructing the tetrapyrrole skeleton through redox reactions[6] and metal-mediated processes.[8] The reaction of dibenzocorrorin (**3**) with copper(II) acetate yields fused product **1**, featuring a distinct nitrogen-embedded [6.5.5.5.7.5.5.5.6]-fused ring structure. Based on nucleus-independent chemical shift (NICS) values, the

[a] *Department of Applied Chemistry, Graduate School of Engineering, Kyushu University, Fukuoka 819-0395 (Japan), E-mail: furuta.hiroyuki.165@m.kyushu-u.ac.jp*
[b] *Department of Chemistry, Graduate School of Sciences, Tokyo Metropolitan University, Tokyo 192-0397 (Japan), E-mail: ishidam@tmu.ac.jp*
[c] *Advanced Research Support Center, Ehime University, Matsuyama 790-8577 (Japan)*
[d] *Institute for Advanced Study, Kyushu University, Fukuoka 819-0395 (Japan), E-mail: yasuda@ifrc.kyushu-u.ac.jp*
† Footnotes relating to the title and/or authors should appear here.
Supplementary Information available: [details of any supplementary information available should be included here]. See DOI: 10.1039/x0xx00000x

local diazadicyclopenta[*cd,ij*]azulene unit exhibits an antiaromatic character of the nitrogen-containing expanded azulene fragment in the structure (Fig. 1e).

This product can be classified as polycyclic antiaromatic hydrocarbons (PAAHs), which have garnered significant attention due to their unique electronic properties and potential applications in various fields. The incorporation of multiple pyrrole units introduces an intrinsically stable 4nπ antiaromatic character into planar PAH scaffolds (e.g., *s*-indacene (**4**), diazapyracylene (**5**), and azacorronene (**6**); Fig. 1b).[9] These compounds, expected to function as semiconductor materials, exhibit unique electron donor-acceptor characteristics due to their high HOMO and low LUMO energy levels. Although antiaromatic compounds were long predicted to display ambipolar charge-transport characteristics, their instability has historically limited their investigation.[10] In this context, the coplanar nitrogen-embedded fused structure of **1** is particularly noteworthy, offering distinct second near-infrared (NIR-II) optical properties, facile redox reactivity, and enhanced charge-transport capabilities.

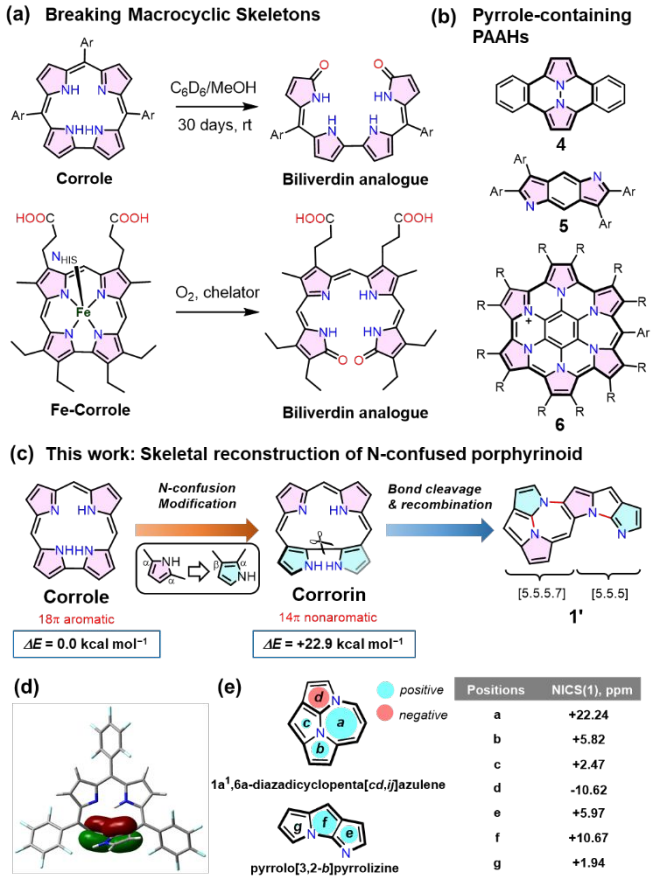

Fig. 1 (a) Representative reactions for destructive macrocycles of corroles. (b) Chemical structures of the family of the pyrrole-containing polycyclic antiaromatic hydrocarbons **4**–**6**. (c) Schematic illustration of the design strategy for pyrrole-embedded polycyclic molecules **1'** through the destruction of tetrapyrrole macrocycles. The thermal stabilities (kcal mol^{-1}) of corrole and corrorin skeletons were obtained by B3LYP-D3/6-311G(d,p) level calculation. (d) NBO analysis of corrorin originated from the interaction between the π-orbital overlap of the bipyrrole moiety. (e) NICS(1) values of the fragments units of **1'** and electrostatic potential map of **1'** obtained by B3LYP-D3/6-311G(d,p) calculations. Isovalues are set to 0.02, and the blue and red colours indicate positive and negative potentials, respectively.

Results and discussion

The precursor for dibenzocorrorin **3** was synthesized following a previously reported procedure.[11] Pyrrole-embedded polycyclic compounds were synthesized through the oxidative degradation of the carbacorrole analogue **3** and subsequent multiple C–N fusion reactions (Fig. 2a). Treatment of **3** with copper(II) acetate in a pyridine solution resulted in the formation of multiple products within 3 hours under ambient conditions. Following purification by silica gel column chromatography, two primary products were successfully isolated with yields of 28% and 3%, respectively. The first brown fraction displayed a fast atom bombardment (FAB) mass signal at 892.0746 (Fig. S7, see Electronic supplementary information (ESI)), suggesting a minor proton loss from the original **3** and indicating skeletal fusion. In the case of the second product, an increased mass peak at 1782.1333 was observed, indicating a possible dimeric form of the tetrapyrrolic **1** (Fig. S8).

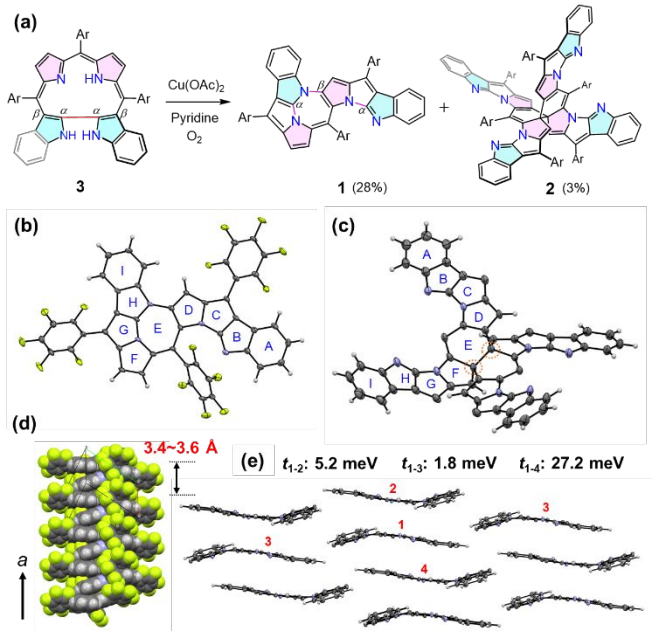

Fig. 2 (a) Synthesis of polycyclic compounds **1** and **2** by oxidative destruction of **3**. Crystal structures of (b) **1** and (c) **2** are shown (top views) with thermal ellipsoids at 50% probability. Solvent molecules and C_6F_5-*meso*-substituents are omitted for clarity in the view of **2**. Spiro-carbon atoms in **2** are highlighted by an orange circle. (d) Packing structure of **1** along with the a-axis. (e) Charge transfer integral (*J*, in meV) calculated from the HOMOs for the nearest intralayer neighbours in the crystal structure of **1** based on the PW-91/TZP level calculation.

To unveil the unique structures of the products, we conducted X-ray diffraction analysis on single crystals **1** and **2**, obtained through recrystallization from mixed solvents ($CHCl_3$/hexane) (Fig. 2b–c and Table S2 in ESI).[12] The structure of needle-shaped crystal **1** revealed a sequential [6.5.5.5.7.5.5.5.6]-fused ring core containing the multiply C–N bonded structure. The core geometry of **1** exhibited a slight bend, possibly due to intermolecular interactions. In the

packing structure of **1**, each polycyclic core moiety slip-stacked in an antiparallel manner along the a-axis, with a mean plane distance of approximately 3.4~3.6 Å (Fig. 2d). The *meso*-aryl-substituents at the C and G rings exhibited relatively low dihedral angles to the mean plane, measuring 37.5° and 41.7°, respectively. This orientation may facilitate intermolecular stacking, as depicted in the Hirshfeld surface plot (Fig. S9). For compound **2**, in line with the mass spectral results, confirmation of the dimeric form of the fused tetrapyrrole core was achieved (Fig. 2c). Similar to **1**, the C–N bond formation between the pyrrole N and indole α-C was evident. Additionally, pyrrole β-carbons were connected to form a new six-membered ring (E) through two spiro-sp^3-carbon bridges. The resulting cross-linked boomerang-shaped ring system exhibited quasi-perpendicular orientation due to shared spiro-carbon atoms, leading to distinct optical properties (Fig. S10 and S13).

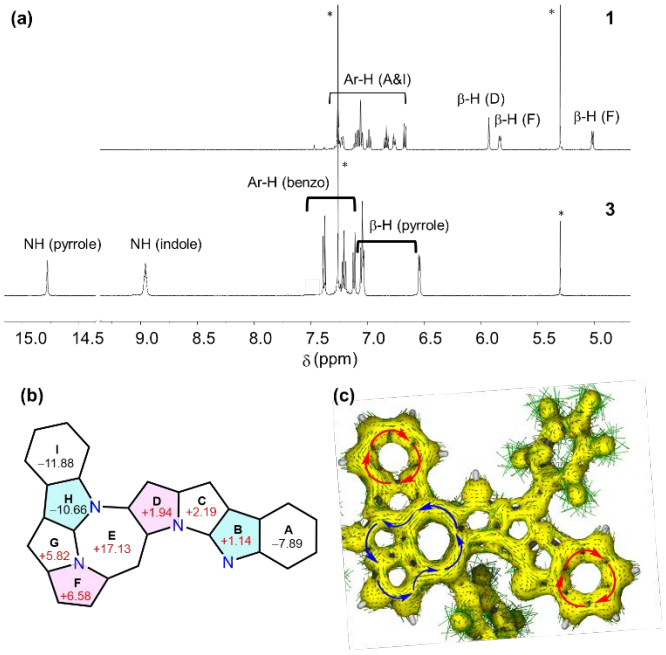

Fig. 3 (a) Comparative ^{1}H-NMR spectrum of **1** (top) determined in $CDCl_3$ with that of **3** (bottom). Labels of the NHs and CHs of the ring units can be referred from the structure given in (b). The asterisks indicated the residual solvent peaks. (b) NICS(1) values and (c) ACID plot (isosurface values of 0.05) of the core for **1** obtained by B3LYP/6-311G(d,p) level calculations.

While the exact mechanism behind the formation of **1** and **2** remains unclear, a plausible scheme is presented in Scheme S1. Optimization of the reaction conditions highlighted the crucial role of copper(II) salt in product formation rather than other potential metal salts (Entries 1–7, Table S1). Additionally, the basic solvent, pyridine, was found to be necessary to promote deprotonation (Entries 8–11, Table S1). The electron paramagnetic resonance (EPR) spectrum of the reaction solution of **3** suggested the formation of a copper(II) complex during the reaction (Fig. S12). The relatively strained C_α–C_α bond neighboring the inner dipyrrin site may be selectively activated (Scheme S1).[13] Based on the observed structure, chelation-assisted copper(II)-mediated C_α–C_α bond cleavage and subsequent recombination of the C_α–N bonds resulted in the polycyclic fused products.

The ^{1}H-NMR spectrum of **1** supported the low symmetric polycyclic structure (Fig. 3a). In comparison to the spectrum of **3**, the loss of three pyrrole NH signals, as well as a β-pyrrole proton, was observed in the low-field region. Notably, two doublet signals assigned to the β-protons of the ring F appeared at 5.01 and 5.83 ppm, considerably high-field shifted. To analyze the hidden open-shell electronic contribution, variable-temperature ^{1}H-NMR spectra of **1** were measured in $C_2D_2Cl_4$ (Fig. S11). Upon increasing the temperature (up to +100 °C), a slight broadening of the CH signals was observed; however, no significant peak shifts occurred. In addition, the broken symmetry UDFT calculations resulted in the ground closed-shell electronic structures. These results indicate a negligible contribution from the open-shell species (e.g., diradicaloids).[14]

To gain insight into the local aromaticity of the core structure of **1**, nuclear independent chemical shift (NICS)[15] values and anisotropy of the induced current density (ACID)[16] plots were analyzed based on the B3LYP calculation (Fig. 3b–c). Interestingly, the NICS(1) values at the center of E, F, and G rings were positive, especially at the seven-membered ring E (+17.13 ppm). Consistently, the counterclockwise ring current was visualized at the fused rings E–G moiety in the ACID plot. Further, the strongly deshielded iso-chemical shielding surface $(ICSS(1)_{zz})$[17] maps of **1** around E, F, and G rings supported the above observations (Fig. S16). The characteristic antiaromatic feature of the diazadicyclopenta[*cd,ij*]azulene fragment was also demonstrated by NICS and ACID plot analyses (Fig. S15a). These results suggest the presence of the partial paratropic ring current in **1**, which is consistent with the observation in the ^{1}H-NMR spectrum. In the resting pyrrolo[3,2-*b*]pyrrolizine fragment (ring B,C,D), the presence of the potential paratropic ring current is expected, as inferred from DFT calculations (Fig. S15b). However, the peripheral fusion of the diazadicyclopentaazulene and benzene moieties gave rise to a lesser magnitude of the paratropic ring current in **1** due to electronic perturbation, as inferred from NICS scan up to 5 Å above and below the plane of the rings A to I (Fig. S17).[18]

The distinctive electronic structure of **1** is evident in its low-energy second near-infrared-II (NIR-II) absorption in CH_2Cl_2, indicating a narrow HOMO–LUMO energy gap (Fig. 4a).[19] The molecular orbital (MO) diagram of **1**, calculated using the B3LYP method, reveals the π-delocalized HOMO and LUMO (Fig. 4c). The broken degeneracy of the frontier HOMO and LUMO pair (e.g., H/H-1 and L/L+1) induces a partially allowed HOMO–LUMO transition with an oscillator strength (*f*) of 0.1 at 1340 nm, as determined by time-dependent (TD) DFT calculation (Fig. S18). The shoulder absorption around 572 nm corresponds to the HOMO-2 to LUMO transition.

The cyclic voltammogram of **1**, measured in CH_2Cl_2 containing 0.1 M *n*-tetrabutylammonium hexafluorophosphate electrolyte, exhibits two independent oxidation waves at 0.15 and 0.57 V (vs. ferrocene/ferrocenium couple), as well as two reduction waves at −1.00 and −1.35 V (Fig. 4b). These values

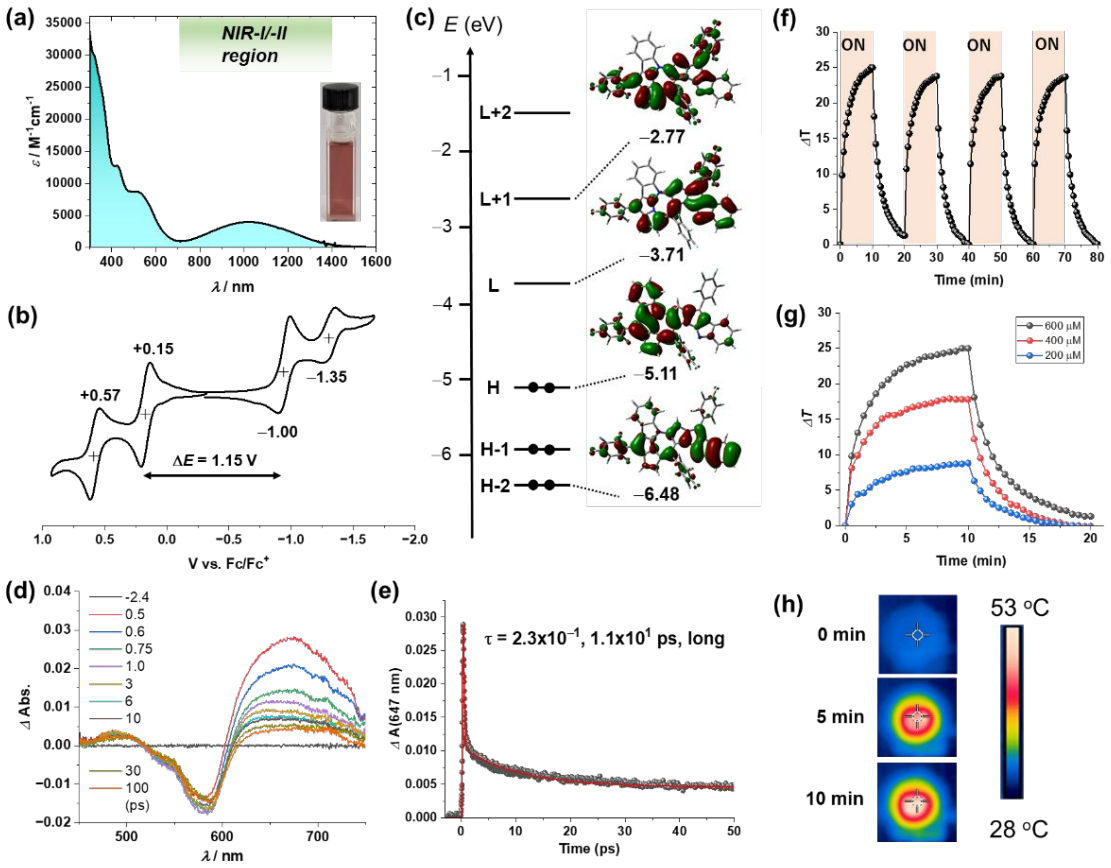

Fig. 4 (a) UV-vis-NIR absorption spectrum of **1** recorded in CH_2Cl_2. Inset shows a photo of the solution under ambient light. (b) Cyclic voltammogram of **1** determined in CH_2Cl_2 containing 0.1 M *n*-tetrabutylammonium hexafluorophosphate as an electrolyte. Scan rate = 0.1 V/s. (c) MO energy diagram of **1** obtained by B3LYP/6-311G(d,p) level calculation. (d) fs-Transient absorption spectra and (e) decay time profile of **1** in toluene upon photoexcitation at 400 nm. (f) Temperature changes of the solution containing **1** under laser ON/OFF cycles of NIR laser at 940 nm irradiation. (g) Temperature changes of the solution containing **1** at various concentrations under NIR laser irradiation for 10 min. (h) Thermography images of the toluene solution of **1**.

indicate relatively facile oxidative reactivity and a narrow electrochemical energy gap of 1.15 V, consistent with the corresponding HOMO–LUMO gap observed in the optical study. Furthermore, to investigate the excited-state dynamics, femtosecond (fs) transient absorption (TA) spectra of **1** were recorded in toluene (Fig. 4d). Upon excitation at 400 nm, the fs-TA spectra of **1** displayed a broad excited-state absorption (ESA) band at 670 nm and a ground-state bleaching (GSB) band at 580 nm. The bi-exponential decay profile of **1** revealed an ultrashort S_1 state lifetime of 11.09 ps, consistent with the relaxation behaviour of typical antiaromatic compounds.[20] The results support the nonemissive nature of **1**, and a small contribution from the minor long-lived species, probably originating from the triplet state, can be anticipated.

Based on the intriguing NIR optical feature along with the ultrashort S_1 state dynamics, the photothermal conversion capability of **1** was explored under laser irradiation at 940 nm (Fig. 4f–h). Several NIR-II molecular materials have been proposed for applications in photothermal therapy of noninvasive cancer treatment.[21] Antiaromatic molecules have been less explored as potential photothermal therapeutic agents due to their intrinsic optically forbidden transitions in the NIR window and low photostability. Here, we tested the efficiency of **1** in toluene solution, and the drastic temperature change (ΔT) of the solution was found to be up to 25 ˚C, as evidenced by the thermal images (Fig. 4h). The extent of the temperature increase depends on the concentration of **1**, while a negligible temperature rise was observed under similar conditions without the dyes (Fig. 4g). Notably, despite the intrinsic antiaromatic character, the high photostability of **1** was determined by its excellent heating/cooling reproducibility (Fig. 4f). Based on the time constants (τ_s) for heat transfer of the system, the efficiency (η) of compound **1** is found to be 31%.

To examine the intrinsic charge-transport properties of **1**, single-crystal organic field-effect transistor (OFET) devices were fabricated in a top-contact/bottom-gate configuration (Fig. 5a). Suitable needle crystals were grown by drop-casting the solution onto octyl trichlorosilane (OTS)-treated SiO_2 substrates in a nitrogen atmosphere. Then, gold electrodes were deposited onto each single crystal to measure the output and transfer characteristics (Fig. 5b). As a result, distinct p-type FET responses with a hole mobility (μ_h) of 3.6×10^{-3} cm^2 V^{-1} s^{-1} were observed for the device. In comparison to the hole mobilities of PAHs containing antiaromatic segments, such as cyclopenta[pqr]indeno[2,1,7-*ijk*]tetraphene ($\mu_h \sim 5.0 \times 10^{-3}$ cm^2 V^{-1} s^{-1}), hexa-xylyl *s*-indacene ($\mu_h \sim 1.05 \times 10^{-2}$ cm^2 V^{-1} s^{-1}),

sulfur-bridged tetrathienylene (μ_h = 0.40 cm^2 V^{-1} s^{-1}), the moderate OFET properties of crystalline **1** could be attributed to the less ideal overlap of the molecular core surrounded by aryl substituents.[22] Though the molecules are slip-stacked along the longer needle axial (Fig. 2d), the charge transfer integrals (*J*) of the hole transport in the stacked configuration are not remarkable due to the presence of the pairs of dimeric **1** in the packing column domains (Fig. 2e).

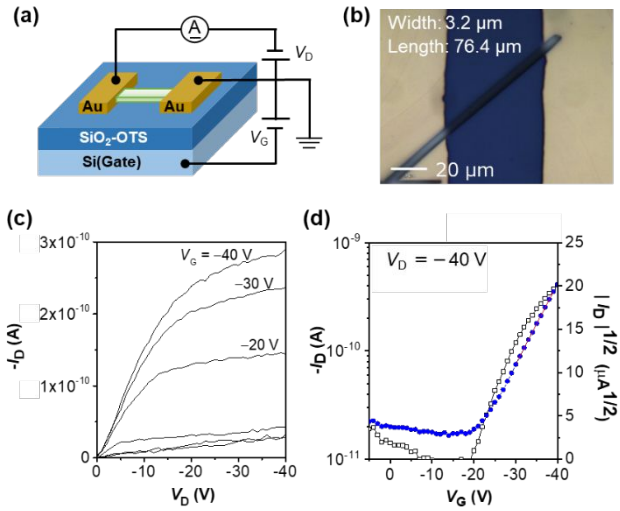

Fig. 5 (a) Schematic illustration of a single-crystal OFET. (b) Microscopic image of the device using a microneedle **1**; the channel width and length are given. (c) Output and (d) transfer curves of the single-crystal OFET of **1**.

Experimental

Synthesis of 1 and 2.

Compound **3** (11.2 mg, 0.0125 mmol) was dissolved in 5 mL pyridine, and $Cu(OAc)_2$ (12.4 mg, 0.0670 mmol) was added to the mixture. After stirring for 3 h, the reaction mixture was diluted with CH_2Cl_2, washed with H_2O, and the resulting organic layer was collected and dried over anhydrous Na_2SO_4. The filtrate was evaporated under reduced pressure. Purification by silica gel column chromatography using CH_2Cl_2/Hexane = 20/80 (*v/v*) as eluent afforded the desired product **1** in 28% yield (3.2 mg, 0.0036 mmol) as brown solid, and **2** in 3% yield as gray solid.

Data for **1**: ^{1}H-NMR ($CDCl_3$, 495 MHz, ppm): δ 7.22 (d, *J* = 7.9 Hz, 1H), 7.13 – 7.03 (m, 3H), 6.99 (td, *J* = 7.7, 1.0 Hz, 1H), 6.86 – 6.81 (m, 1H), 6.76 (d, *J* = 7.2 Hz, 1H), 6.67 (d, *J* = 7.6 Hz, 1H), 5.93 (s, 1H), 5.83 (d, *J* = 5.7 Hz, 1H), 5.02 (d, *J* = 5.7 Hz, 1H). ^{19}F-NMR ($CDCl_3$, 466 MHz, ppm): δ −134.84 (d, *J* = 16.0 Hz, 2F), −138.24 (dd, *J* = 23.1, 6.9 Hz, 2F), −138.61 (dd, *J* = 22.7, 7.0 Hz, 2F), −148.95 (t, *J* = 21.0 Hz, 1F), −154.86 (t, *J* = 20.8 Hz, 1F), −156.58 (t, *J* = 20.7 Hz, 1F), −159.05 (qd, *J* = 10.4, 5.2 Hz, 2F), −161.91 (td, *J* = 22.1, 7.6 Hz, 2F), −162.51 (dt, *J* = 22.9, 6.9 Hz, 2F). HRMS (FAB): *m/z* = 892.0744 (found); 892.0744 (calcd. For $C_{45}H_{11}F_{15}N_4$, Error: −0.1 ppm).

Data for **2**: ^{1}H-NMR (CD_2Cl_2, 495 MHz, ppm): *δ* 7.36 – 7.32 (m, 2H), 7.29 (d, *J* = 7.3 Hz, 2H), 7.09 (d, *J* = 7.8 Hz, 2H), 7.01 (t, *J* = 7.3 Hz, 2H), 6.98 – 6.94 (m, 2H), 6.82 – 6.76 (m, 6H), 6.29 (s, 2H), 6.03 (s, 2H). ^{19}F-NMR (CD_2Cl_2, 466 MHz, ppm): *δ* −135.12 (d, *J* = 17.3 Hz, 4F), −136.63 (d, *J* = 17.6 Hz, 4F), −138.11 (d, *J* = 23.8 Hz, 2F), −141.21 (dd, *J* = 23.3, 6.6 Hz, 2F), −150.48 (t, *J* = 20.8 Hz, 2F), −150.80 (t, *J* = 20.8 Hz, 2F), −156.87 (t, *J* = 20.7 Hz, 2F), −160.39 (t, *J* = 18.3 Hz, 4F), −160.71 (dt, *J* = 20.3, 10.1 Hz, 4F), −165.14 - −165.37 (m, 2F), −166.25 (td, *J* = 22.6, 6.8 Hz, 2F). HRMS (FAB): *m/z* =1782.1333 (found); 1782.1332 (calcd. For $C_{90}H_{20}F_{30}N_8$; Error: +0.1 ppm).

Conclusions

This study presents a novel synthetic approach for creating nitrogen-embedded polycyclic molecules **1** and **2** through the destruction and reformation of the macrocyclic π-conjugated corrole isomer **3**. Utilizing various spectroscopic techniques, including NMR and theoretical calculations, the influence of the 12π-antiaromatic ring contributor was elucidated in the electronic structure **1**. The presence of characteristic NIR-II absorption, an ultrashort excited-state lifetime, and a narrow electrochemical energy gap further supported the intrinsic structure of **1**. Despite its antiaromatic character, compound **1** exhibited high photostability, as determined in the NIR photothermal conversion study. Moreover, the stacked packing feature of crystalline **1** demonstrated hole transport capability in the OFET device. These insights open avenues for designing high-performance light-responsive organic materials (e.g., NIR-photo detectors[23]) using a tetrapyrrole-based molecular platform.

Author contributions

[#]B.B. and S.Y. contributed equally to the work.

Conflicts of interest

There are no conflicts to declare.

Data availability

The data supporting this article have been included in the electronic supplementary information.

Acknowledgements

The authors acknowledge the support from Grant-in-Aid for Scientific Research and Exploratory Research; JP22K19937 (M.I.), JP21H04694 (T.Y.), JP20H02802 (D.K.), from JSPS, a JST PRESTO: JPMJPR2103 (M.I.), and the Izumi science and technology foundation (M.I.). Part of the work was using research equipment shared in the MEXT Project to promote public utilization of advanced research infrastructure (Program supporting the introduction of the new sharing system) Grant Number JPMXS0422300120. The author also thanks Prof. K. Tanaka (Kyushu Univ.) for allowing us to measure the femtosecond TA spectroscopic system and Prof. K. Sugiura (Tokyo Metropolitan Univ.) for the fruitful discussion.

Notes and references

1 (*a*) Y. Shi, F. Zhang and R. J. Linhardt, Porphyrin-based compounds and their applications in materials and in medicine, *Dyes Pigm.*, 2021, **188**, 109136; (*b*) S. R. D. Gamelas, J. P. C. Tomé, A. C. Tomé and L. M. O. Lourenço, Porphyrin-containing materials for photodegradation of organic pollutants in wastewaters: a review, *Catal. Sci. Technol.,* 2024, **14**, 2352; (*c*) A. Mahmood, J.-Y. Hu, B. Xiao, A. Tang, X. Wang and E. Zhou, Recent progress in porphyrin-based materials for organic solar cells, *J. Mater. Chem. A*, 2018, **6**, 16769; (*d*) T. Tanaka and A. Osuka, Conjugated porphyrin arrays: synthesis, properties and applications for functional materials, *Chem. Soc. Rev.,* 2015, **44**, 943; (*e*) A. Akbar, S. Khan, T. Chatterjee and M. Ghosh, Unleashing the power of porphyrin photosensitizers: Illuminating breakthroughs in photodynamic therapy, *J. Photochem. Photobiol. B, Biology*, 2023, **248**, 112796.

2 (*a*) W. Suzuki, H. Kotani, T. Ishizuka and T. Kojima, Efficient Photocatalytic CO_2 Reduction by a Ni(II) Complex Having Pyridine Pendants through Capturing a Mg^{2+} Ion as a Lewis-Acid Cocatalyst, *J. Am. Chem. Soc.,* 2019, **141**, 5987; (*b*) K. Rybicka-Jasińska, W. Shan, K. Zawada, K. M. Kadish and D. Gryko, Porphyrins as Photoredox Catalysts: Experimental and Theoretical Studies, *J. Am. Chem. Soc.,* 2016, **138**, 15451; (*c*) J. L. Sessler, S. K. Kim, D. E. Gross, C.-H. Lee, J. S. Kim and V. M. Lynch, Crown-6-calix[4]arene-Capped Calix[4]pyrrole: An Ion-Pair Receptor for Solvent-Separated CsF Ions, *J. Am. Chem. Soc*., 2008, **130**, 13162; (*d*) M. K. Chahal, A. Liyanage, H. B. Gobeze, D. T. Payne, K. Ariga, J. P. Hill and F. D'Souza, Supramolecular ultrafast energy and electron transfer in a directly linked BODIPY–oxoporphyrinogen dyad upon fluoride ion binding, *Chem. Commun*., 2020, **56**, 3855; (*e*) E. Clo, J. W. Snyder, N. V. Voigt, P. R. Ogilby and K. V. Gothelf, DNA-programmed control of photosensitized singlet oxygen production, *J. Am. Chem. Soc.,* 2006, **128**, 4200; (*f*) J. Kralova, M. Kolar, M. Kahle, J. Truksa, S. Lettlova, K. Balusikova and P. Bartunek, Glycol porphyrin derivatives and temoporfin elicit resistance to photodynamic therapy by different mechanisms, *Sci. Rep.*, 2017, **7**, 44497; (*g*) T. Haino, T. Fujii, A. Watanabe and U. Takayanagi, Supramolecular polymer formed by reversible self-assembly of tetrakisporphyrin, *Proc. Natl. Acad. Sci. USA*, 2009, **106**, 10477.

3 (*a*) J. F. B. Barata, M. Graça P. M. S. Neves, M. A. F. Faustino, A. C. Tomé and J. A. S. Cavaleiro, Strategies for Corrole Functionalization, *Chem. Rev.,* 2017, **117**, 3192; (*b*) C. D. Natale, C. P. Gros and R. Paolesse, Corroles at work: a small macrocycle for great applications, *Chem. Soc. Rev*., 2022, **51**, 1277; (*c*) A. Kumar, D. Kim, S. Kumar, A. Mahammed, D. G. Churchill and Z. Gross, Milestones in corrole chemistry: historical ligand syntheses and post-functionalization, *Chem. Soc. Rev*., 2023, **52**, 573.

4 (*a*) T. Matsui, M. Unno and M. Ikeda-Saito, Heme oxygenase reveals its strategy for catalyzing three successive oxygenation reactions, *Acc. Chem. Res*., 2010, **43**, 240; (*b*) T. Mizutani, Coupled oxidation of iron tetraarylporphyrins as a synthetic tool for linear tetrapyrroles, *J. Porphyrins Phthalocyanines,* 2016, **20**, 108.

5 (*a*) R. Orłowski, D. Gryko and D. T. Gryko, Synthesis of corroles and their heteroanalogs, *Chem. Rev*., 2017, **117**, 3102; (*b*) B. Gisk, F. Brégier, R. A. Krüger, M. Bröring and N. Frankenberg-Dinkel, Enzymatic ring opening of an iron corrole by plant-type heme oxygenases: unexpected substrate and protein selectivities, *Biochemistry,* 2010, **49**, 10042; (*d*) C. P. Gros, J.-M. Barbe, E. Espinosa and R. Guilard, Room-temperature autoconversion of free-base corrole into free-base porphyrin, *Angew. Chem., Int. Ed.,* 2006, **45**, 5642; (e) Q. Li, M. Ishida, Y. Wang, C. Li, G. Baryshnikov, B. Zhu, F. Sha, X. Wu, H. Ågren, H. Furuta and Y. Xie, Antiaromatic Sapphyrin Isomer: Transformation into Contracted Porphyrinoids with Variable Aromaticity, *Angew. Chem., Int. Ed.,* 2023, **62**, e202212174.

6 (*a*) M. Toganoh and H. Furuta, Creation from Confusion and Fusion in the Porphyrin World-The Last Three Decades of N-Confused Porphyrinoid Chemistry, *Chem. Rev*., 2022, **122**, 8313; (*b*) M. Pawlicki, I. Kańska and L. Latos-Grażyński, Copper (II) and copper (III) complexes of pyrrole-appended oxacarbaporphyrin, *Inorg. Chem*., 2007, **46**, 6575; (*c*) B. Szyszko, L. Latos-Grażyński and L. Szterenberg, Toward aceneporphyrinoids: synthesis and transformations of palladium (ii) meso-anthriporphyrin, *Chem. Commun*., 2012, **48**, 5004; (*d*) H. Furuta, H. Maeda and A. Osuka, Regioselective oxidative liberation of aryl-substituted tripyrrinone metal complexes from N-confused porphyrin, *Org. Lett.,* 2002, **4**, 181; (*e*) F. Bischoff, A. Riss, G. S. Michelitsch, J. Ducke, J. V. Barth, K. Reuter and W. Auwärter, Surface-mediated ring-opening and porphyrin deconstruction via conformational distortion, *J. Am. Chem. Soc.,* 2021, **143**, 15131; (*f*) K. Zhang, P. Wei, X. Li, H. Ågren and Y. Xie, Oxidative ring closure and metal triggered ring opening: syntheses of macrocyclic and linear hexapyrroles, *Org. Lett*., 2014, **16**, 6354.

7 A. E. Reed, A. L. Curtiss and F. Weinhold, Intermolecular interactions from a natural bond orbital, donor-acceptor viewpoint, *Chem. Rev.*, 1988, **88**, 899.

8 (*a*) H. Furuta, H. Maeda and A. Osuka, Oxyindolophyrin: A novel fluoride receptor derived from N-confused corrole isomer, *J. Am. Chem. Soc*., 2001, **123**, 6435; (*b*) Y. Xu, B. Zhu, Q. Li, F. Sha, G. Baryshnikov, L. He, Y. Feng, J. Tang, Y. Wei, C. Li, X. Wu, H. Ågren and Y. Xie, Pyrrolylmethylene Appended Corrorin: Peripheral Coordination and Transformation to Pyridyl Incorporated Hemiporphycene Analogue, *Org. Lett.,* 2023, **25**, 1793.

9 (*a*) Y. Morimoto, Y. H. Koo, K. Otsubo, H. Kitakado, S. Seki, A. Osuka and T. Tanaka, Dibenzodiazapyracylenes: Doubly N‐Doped Cyclopenta-Fused Polycyclic Molecules That Exhibit High Carrier Mobility, *Angew. Chem., Int. Ed.,* 2022, **61**, e202200341; (*b*) K. Hanida, J. Kim, N. Fukui, Y. Tsutsui, S. Seki, D. Kim and H. Shinokubo, Antiaromatic 1,5-Diaza-s-indacenes, *Angew. Chem., Int. Ed.,* 2021, **60**, 20765; (*c*) K. Oki, M. Takase, S. Mori, A. Shiotari, Y. Sugimoto, K. Ohara, T. Okujima and H. Uno, Synthesis and isolation of antiaromatic expanded azacoronene via intramolecular vilsmeier-type reaction, *J. Am. Chem. Soc*., 2019, **141**, 16255.

10 T. Higashino, and T. Mori, Small-molecule ambipolar transistors, *Phys. Chem. Chem. Phys*., 2022, **24**, 9770.

11 B. Basumatary, I. Hashiguchi, S. Mori, S. Shimizu, M. Ishida and H. Furuta, Copper 1, 19-Diaza-21, 24-dicarbacorrole: A Corrole Analogue with an N–N Linkage Stabilizes a Ground-State Singlet Organocopper Species, *Angew. Chem., Int. Ed*., 2020, **59**, 15897.

12 Deposition numbers 2327547 (**1**) and 2327548 (**2**) contain the supplementary crystallographic data for this paper. These data are provided free of charge by the joint Cambridge Crystallographic Data Centre and Fachinformationszentrum Karlsruhe Access Structures service.

13 (*a*) G. Fumagalli, S. Stanton and J. F. Bower, Recent methodologies that exploit C–C single-bond cleavage of strained ring systems by transition metal complexes, *Chem. Rev*., 2017, **117**, 9404; (*b*) M. Murakami and N. Ishida, Potential of metal-catalyzed C–C single bond cleavage for organic synthesis, *J. Am. Chem. Soc*., 2016, **128**, 13759; (*c*) X. Wang, N. Li, Z. Li and H. Rao, Copper-Catalyzed Dehydrogenative C(sp^2)–N Bond Formation via Direct Oxidative Activation of an Anilidic N–H Bond: Synthesis of Benzoimidazo[1,2-a]indoles, *J. Org. Chem.*, 2017, **82**, 10158.

14 (*a*) M. Abe, Diradicals, *Chem. Rev.,* 2013, **113**, 7011; (*b*) J. J. Dressler, M. Teraoka, G. L. Espejo, R. Kishi, S. Takamuku, C. J. Gómez-García, L. N. Zakharov, M. Nakano, J. Casado and M. M. Haley, Thiophene and its sulfur inhibit indenoindenodibenzothiophene diradicals from low-energy lying thermal triplets, *Nat. Chem.,* 2018, **10**, 1134.
15 Z. Chen, C. S. Wannere, C. Corminboeuf, R. Puchta and P. v. R. Schleyer, Nucleus-independent chemical shifts (NICS) as an aromaticity criterion, *Chem. Rev*., 2005, **105**, 3842.
16 R. Herges and D. Geuenich, Delocalization of electrons in molecules, *J. Phys. Chem. A,* 2001, **105**, 3214.
17 (*a*) S. Klod and E. Kleinpeter, Ab initio calculation of the anisotropy effect of multiple bonds and the ring current effect of arenes—application in conformational and configurational analysis, *J. Chem. Soc., Perkin Trans. 2*, 2001, 1893; (*b*) T. Lu and F. Chen, Multiwfn: A multifunctional wavefunction analyzer *J. Comput. Chem*., 2012, **33**, 580.
18 J. Usuba and A. Fukazawa, Thiophene ‐ Fused 1, 4 ‐ Diazapentalene: A Stable C= N ‐ Containing π ‐ Conjugated System with Restored Antiaromaticity, *Chem.–Eur. J*., 2021, **27**, 16127.
19 Z. Feng, T. Tang, T. Wu, X. Yu, Y. Zhang, M. Wang, J. Zheng, Y. Ying, S. Chen, J. Zhou, X. Fan, D. Zhang, S. Li, M. Zhang and J. Qian, Perfecting and extending the near-infrared imaging window, *Light Sci. Appl*., 2021, **10**, 197.
20 (*a*) J. Liu, J. Ma, K. Zhang, P. Ravat, P. Machata, S. Avdoshenko, F. Hennersdorf, H. Komber, W. Pisula, J. J. Weigand, A. A. Popov, R. Berger, K. Müllen and X. Feng, π-extended and curved antiaromatic polycyclic hydrocarbons, *J. Am. Chem. Soc*., 2017, **139**, 7513; (*b*) S.-J. Jhang, J. Pandidurai, C.-P. Chu, H. Miyoshi, Y. Takahara, M. Miki, H. Sotome, H. Miyasaka, S. Chatterjee, R. Ozawa, Y. Ie, I. Hisaki, C.-L. Tsai, Y.-J. Cheng and Y. Tobe, s-Indacene Revisited: Modular Synthesis and Modulation of Structures and Molecular Orbitals of Hexaaryl Derivativesa, *J. Am. Chem. Soc*., 2023, **145**, 4716; (*c*) T. Nishinaga, T. Ohmae, K. Aita, M. Takase, M. Iyoda, T. Arai and Y. Kunugi, Antiaromatic planar cyclooctatetraene: a strategy for developing ambipolar semiconductors for field effect transistors, *Chem. Commun.,* 2013, **49**, 5354.
21 (*a*) H. S. Jung, P. Verwilst, A. Sharma, J. Shin, J. L. Sessler and J. S. Kim, Organic molecule-based photothermal agents: an expanding photothermal therapy universe, *Chem. Soc. Rev*., 2018, **47**, 2280; (*b*) Y. Liu, P. Bhattarai, Z. Dai and X. Chen, Photothermal therapy and photoacoustic imaging via nanotheranostics in fighting cancer, *Chem. Soc. Rev*., 2019, **48**, 2053; (*c*) S. Lv, Y. Miao, D. Liu and F. Song, Recent development of photothermal agents (PTAs) based on small organic molecular dyes, *ChemBioChem,* 2020, **21**, 2098.
22 (*a*) J. Oh, Y. M. Sung, Y. Hong and D. Kim, Spectroscopic diagnosis of excited-state aromaticity: capturing electronic structures and conformations upon aromaticity reversal, *Acc. Chem. Res*., 2018, **51**, 1349; (*b*) J. Kim, J. Oh, A. Osuka and D. Kim, Porphyrinoids, a unique platform for exploring excited-state aromaticity, *Chem. Soc. Rev.,* 2022, **51**, 268.
23 Q. Li, Y. Guo and Y. Liu, Exploration of near-infrared organic photodetectors, *Chem. Mater*., 2019, **31**, 6359.

The data supporting this article have been included as part of the Supplementary Information.